



Assessing the Mineral Alteration in Ambaji–Deri Region (Northwestern India) Using Hyperspectral Remote Sensing

Parth Samani¹ · S. P. Prizomwala¹ · A. S. Rajawat²

Received: 26 May 2019 / Accepted: 9 October 2020 / Published online: 17 October 2020
© Indian Society of Remote Sensing 2020

Abstract

We used Airborne Visible Infrared Imaging Spectrometer-Next Generation data for mapping possible mineral alterations, which aid in mineral exploration over larger areas. The data were subjected to various advanced processing techniques like Minimum Noise Fraction, Pixel Purity Index, *N*-Dimensional visualization and Spectral angle mapper classification. End-member spectra were matched with those of the minerals as available in the United States Geological Survey Spectral Library. In the present study, the Ambaji–Deri area of northwestern India was mapped for mineral alterations. The area has thick forest cover along with rugged topography, which warranted the use of hyperspectral remote sensing approach. The minerals such as calcite, muscovite and chlorite have been mapped, which are showing a good correlation with the ground geological records, barring epidote, whose distribution is scattered. We attribute the possible reason to be the spectral similarities between epidote and chlorite, which makes them difficult to differentiate only on the basis of the present hyperspectral study. The hyperspectral technique, as illustrated, provides powerful tool for mapping mineral alteration to mineral deposits. This enables scrutiny of a wider area of interest to being narrowed down for first-hand field investigations.

Keywords Hyperspectral data · Mineral alteration · Calcite deposits · Remote sensing · Ambaji · India

Introduction

Rapid industrialization, infrastructural growth and societal needs have concerned the mineral wealth to be of utmost importance. Mineral exploration has been considered as the backbone for raw materials and industrial growth of a region. The study of mineral alteration to assess the mineral deposit, via remote sensing, has been a widely used approach (Sabins 1999; Goetz 2009; Van der Meer et al. 2012). These mineral alterations can be studied using multispectral (Landsat TM/ETM + and ASTER) and hyperspectral imaging sensors (Sabins 1999; Abrams 2000; Goetz 2009; Van der Meer et al. 2012).

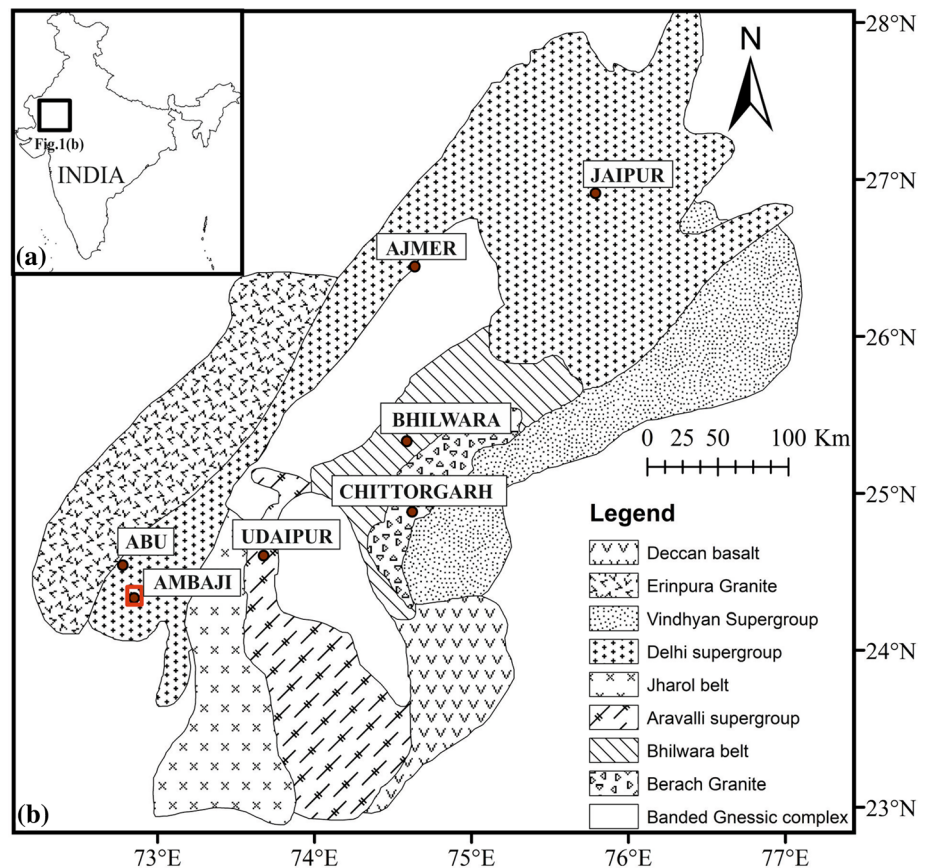
The Landsat Thematic Mapper (TM)/Enhanced Thematic Mapper (ETM +) is often used for mapping mineral alteration, produced due to hydrothermal processes. These mineral alterations can be mapped using band ratio of Band 5 of short-wave infrared (SWIR 1) and Band 7 (SWIR 2) of TM and ETM + (Carranza and Hale 2002; Pour et al. 2017). However, because of the limited band (Band 5 and Band 7) in the SWIR band, Landsat image data cannot effectively resolve the various types of alteration (Crista et al. 2003; Pour and Hashim 2012). ASTER with six spectral bands in the short-wave infrared (SWIR) has the capability to map different alteration minerals in comparison with Landsat Thematic Mapper (TM)/Enhanced Thematic Mapper (ETM +) (Abrams 2000; Crista et al. 2003; Pour and Hashim 2012). For mapping mineral alteration, the most routinely used techniques are the principal component analysis (PCA) and the band ratio techniques. Principal component analysis (PCA) increases the contrast between the bands by decorrelating the band to band information and organizing the data into decreasing signal-to-noise ratio. The resultant increase in contrast will

✉ S. P. Prizomwala
siddharth_prizomwala@yahoo.co.in

¹ Active Tectonics Group, Institute of Seismological Research, Gandhinagar 382009, India

² Geo Sciences Division, Space Applications Centre-ISRO, Ahmedabad, India

Fig. 1 Location map showing the study area. **1a** shows the spatial distribution of the Aravalli belt within India. **1b** shows the stratigraphic succession of Aravalli belt. The box near Ambaji area in Fig. 1b shows the location of study area modified after (Mishra 2015)



highlight the mineral of interest by selecting the appropriate principal component, based on the reflectance and absorption feature of the mineral (Sabins 1999; Crósta et al. 2003; Van der Meer et al. 2012; Pour and Hashim 2012). Band ratio is the technique where the ratio of band corresponding to the reflectance of the targeted mineral and band corresponding to the absorption feature of the same mineral is taken. For example, ASTER Band 7/6 is used to identify the muscovite, whereas Band 8/9 is used to highlight features pertaining to Al–OH vibrations (Pour and Hashim 2015; Pour et al. 2017). However, with fewer bands and the coarser spectral resolution, in SWIR region, the precise mapping of minerals is not possible (Hunt 1979; Mars and Rowan 2006).

Hyperspectral imaging spectroscopy, with its hundreds of narrow and continuous bands, is found to be more efficient in identifying Earth's material, through their spectral signature compared to multispectral imaging sensor (Landsat and ASTER) (Shaw and Burke 2003; Taylor et al. 2007; Goetz 2009; Li et al. 2012; Van der Meer et al. 2012; Krishna Mohan and Porwal 2015; Ramakrishnan and Bharti 2016; Khanna et al. 2018). Out of hundreds of bands, the bands in short-wave infrared (SWIR) region of hyperspectral imaging sensors are very useful for mapping mineral alteration in hydrothermally altered minerals (Laakso et al. 2015; Graham et al. 2017). The hyperspectral

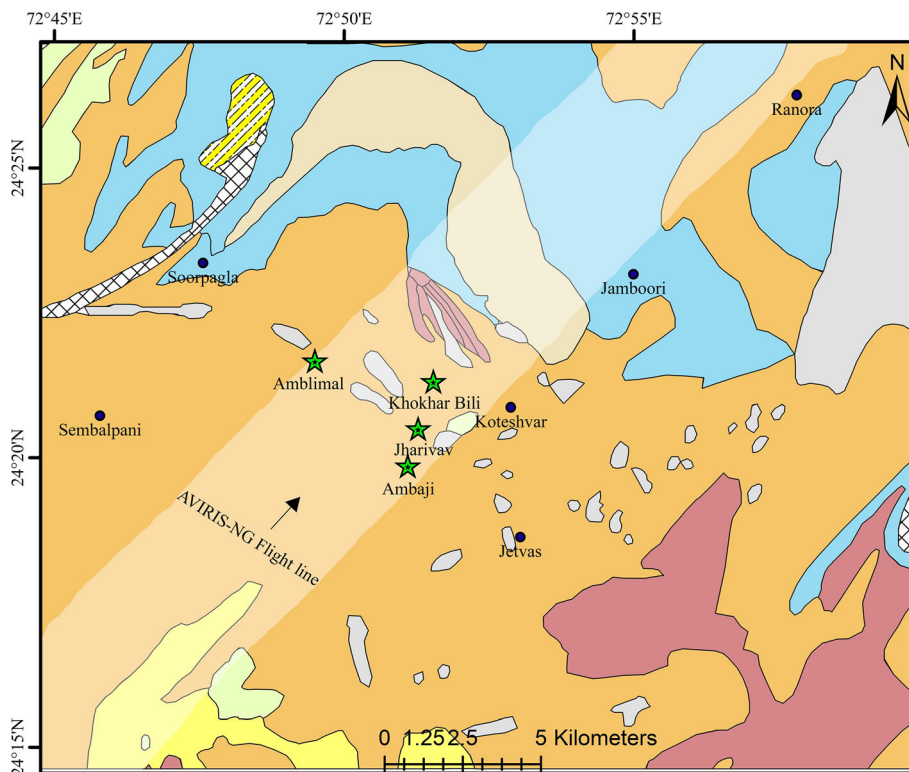
data have been found suitable for identification and exploration of the mineral alterations in Alaska, USA (Kruse et al. 1993; Harraden et al. 2013; Swayze et al. 2014; Kokaly et al. 2016; Graham et al. 2017), Australia (Mauger et al. 2007; Laukamp et al. 2011), Canada (Laakso et al. 2015, 2016), India (Bharti et al. 2015; Bhattacharya et al. 2012; Bharti and Ramakrishnan 2014).

Ambaji–Deri, area located in the western part of India (Fig. 1), is a well-known area for its polymetallic massive sulphide deposits (Deb 1979, 1980; Tiwary and Deb 1997). The area is covered under the forest and has a rugged terrain, owing to which the conventional geological exploration is complicated. Hence, in the present study, we aim to assess the application of hyperspectral remote sensing in mapping of the hydrothermal mineral alteration. This is vital first step for more in-depth mineral exploration in the region.

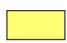






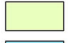





Geological Setup of the Study Area

The Ambaji–Deri area falls under the Delhi supergroup of Aravalli metallogenic province (Gupta et al. 1980; Heron and Ghosh 1938; Porwal et al. 2006). The Delhi supergroup of rocks are of Meso- to Neo-proterozoic in age and contains an arenite-dominated assemblage in the east and a

Fig. 2 Geological map of the area around Ambaji region along with the AVIRIS-NG flight path. It also shows the locations of interest where we found the distribution of alteration minerals after GSI (2012a; b)



Legend

 Recent sediments	 Biotite schist
 Jalor granite	 Calc-Gneiss or schist
 Granite	 Marble
 Biotite schist migmatite	 Calcite marble
 Granite gneiss	 Calc-Gneiss or impure marble
 Epidiorite, hornblende schist, amphibolite	 Location of Interest
 Quartzite	

pelite-dominated assemblage in the west (Fig. 2) (Deb 1979, 1980; Gupta et al. 1980; Heron and Ghosh 1938).

The study area comprises of calcareous, arenaceous and argillaceous meta-sediments belonging to Ajabgarh group of Delhi supergroup (Deb 1979, 1980; Tiwary and Deb 1997; Deb et al. 2001; Porwal et al. 2006). Calcareous meta-sediments like calc-gneiss, calc-silicate dolomite and marble form the basement of the Ajabgarh group. These calcareous sediments are overlain by arenaceous and argillaceous meta-sediments. Concordant bodies of meta-volcanic rocks lie within these meta-sediments. Ajabgarh meta-sediments were intruded by post-Delhi Erinpura granite. This Ajabgarh group has been subjected to the two phase of greenschist facies deformation and thermal metamorphism of hornblende-hornfels facies (Deb 1979, 1980; Tiwary and Deb 1997).

The ore in this region is deposited in the form of massive lenses and tabular bodies (Deb 1979, 1980). These

deposits are hosted by pelitic and psammitic meta-sediments represented by chloritic hornfelses, diopside-forsterite marble, and quartz-mica schists and amphibolite. These deposits are classified under the category of strati-form massive sulphide deposits (Deb 1979, 1980), because the deposits are concordant to the strata of host rock and are in the form of tabular or lensoid bodies. The origin of these deposits is thought to be syngenetic origin based on the various geological evidence, including the poly-metamorphosed nature of the ores (Deb 1979, 1980; Tiwary and Deb 1997).

Methodology

We used the Level-2 (Reflectance) of Airborne Visible Infrared Imaging Spectrometer-Next Generation AVIRIS-NG data, with 425 spectral bands, ranging between 380 and

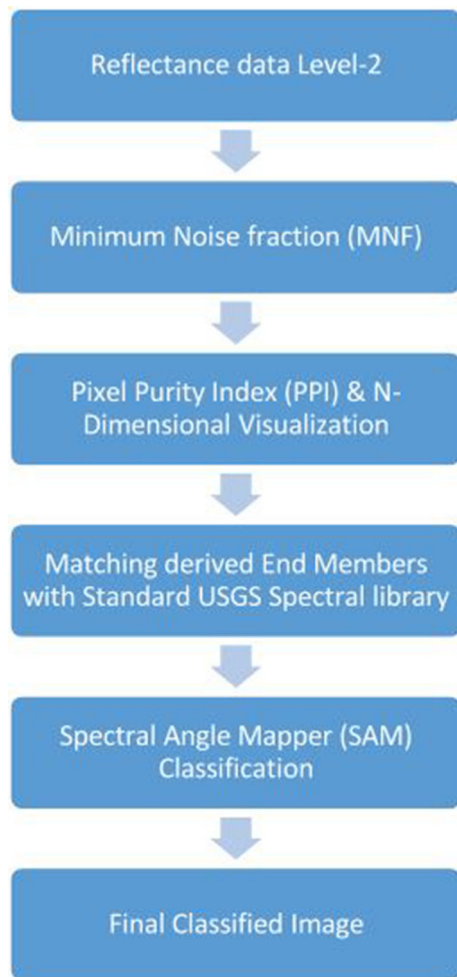


Fig. 3 Flow chart showing the standard protocol for processing the image data modified after Kruse et al. (1993)

2510 nm, with a spectral resolution of 5 nm, spatial resolution of 8.1 mts. The data processing was carried out using Envi software Version 5.1. Since most of the absorption feature of alteration minerals can be diagnosed between 2000 and 2500 nm spectral range (Hunt 1979; Kruse 1988), the data were spectrally subsetting to 110 band out of 425 spectral bands. The spectral range of the subsetting data is 1954.1700 nm to 2500.1201 nm. We followed the standard protocol for data analysis (Fig. 3) (Incorporated Research Systems 2004; Kruse et al. 1993).

Raw data are marred with lot of noise and dimensionality, which hinder the identification of specific minerals (Luo et al. 2016). In order to reduce the dimensionality of the data, Minimum Noise Fraction (MNF) algorithm was used. MNF uses two cascading principal component analysis (PCA), of which the first PCA decorrelates noise from the data and makes it as unit variance (i.e. noise whitening), whereas the second PCA is operated on noise whitened data, this will arrange the data in the decreasing

signal-to-noise ratio with increasing the principal component (Amato et al. 2009; Green et al. 1988).

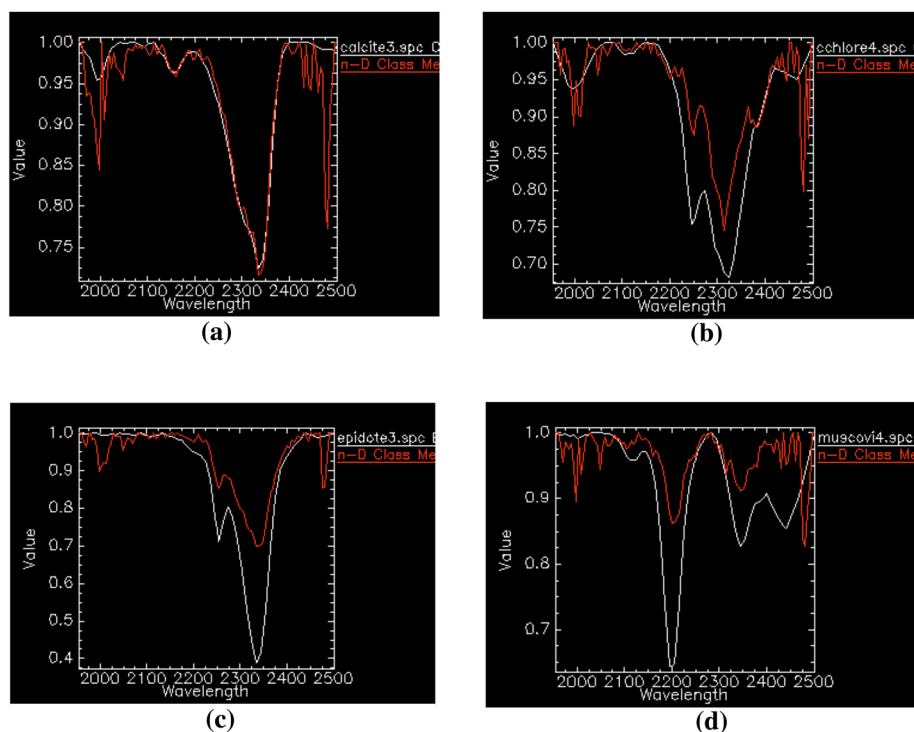
In order to reduce the spatial dimension, the MNF data are further processed for the extraction of the end-members using Pixel Purity Index (PPI) algorithm (Boardman et al. 1993; Wu et al. 2014). The PPI identifies the spectrally unique pixels within the image. These spectrally unique pixels are then used as end-members. It is generally done by projecting pixels on n -dimensional random vectors (Boardman 1994; González et al. 2010). The end-members extracted are then matched with the standard spectral library (USGS mineral library) using spectral analyst tool in Envi software version 5.1 (Nidamanuri and Ramiya 2013). The end-members identified by spectral library match are then used as a trainee for classifying the AVIRIS-NG image data. Finally, Spectral Angle Mapper (SAM) algorithm was used to classify the image data. SAM algorithm classifies the image data by calculating the cosine angle between the reference pixel and the image pixel vector. This method is widely used because of its simplicity and it also nullifies differential illumination effects (Kruse et al. 1993; Nidamanuri and Ramiya 2014).

Results

Data Analysis

The end-members employed for SAM classification contains the spectra of the rock present and were derived from the image data. The results of the end-member spectra matching with the USGS library spectra show the presence of carbonate (CaCO_3), muscovite, chlorite/epidote minerals within the data. The carbonate minerals can be detected based on the absorption feature around 2300 nm, due to vibration of $(\text{CO}_3)^{-2}$ and moreover, the substitution of Ca^{++} and Mg^{++} cations will shift the absorption feature towards 2330 nm, and the presence of Mg will lead it to shift towards 2319 nm, respectively (Gaffey 1987; Laakso et al. 2018). The absorption feature of carbonate in the end-member (Fig. 4a) at 2339 nm suggests the presence of Ca^{++} in cation. Similarly, chlorite feature occurs at 2250 nm due to presence of Fe–O–H and 2340 nm due to presence of Mg–O–H; further it is to be noted that these features vary between 2255 and 2248 nm for absorption centred around 2250 nm and for absorption centre around 2340 nm, they will vary due to variation in Mg^{++} ions (Dalton et al. 2004; Laakso et al. 2016; Neal et al. 2018). The end-member retrieved from image data shows two absorption features, i.e. at 2249 nm and 2339 nm (Fig. 4b). Epidote can be detected by the absorption feature around 2250 nm and 2340 nm due to Fe–O–H and Mg–O–H. It should also be noted that epidote feature can be

Fig. 4 Spectra of end-member derived from the AVIRIS-NG image data were made to match with the known standard library spectra of USGS. Here, **a** represents the calcite mineral which shows the absorption feature at 2339 nm, **b** represents the chlorite mineral which shows the absorption feature at 2249 nm and 2339 nm. **c** represents the epidote mineral which shows absorption feature at 2254 nm and 2339 nm. **d** represents the muscovite mineral which shows the absorption feature 2199 nm



differentiated from chlorite due to presence of deeper absorption feature around 2250 (Neal et al. 2018). Here, the end-member of epidote shows absorption feature at 2254 nm and 2339 nm (Fig. 4c). Muscovite is detected based on 2200 nm due to presence of Al–OH; however, it should be noted that these features also vary between 2199 nm and 2204 due to substitution of Al in the octahedral site of the mica (Hunt 1979; Dalton et al. 2004; Laakso et al. 2015, 2016). In the end-member processed, the value of muscovite is 2199 nm (Fig. 4d), which indicates, according to Laakso et al. (2016), more Al might be present in octahedral site. Confirmation of such results can be done by geochemical studies of rock samples, however, which is not in scope of the present study.

Spatial Distribution of Mineral Alterations and Calcite Marble

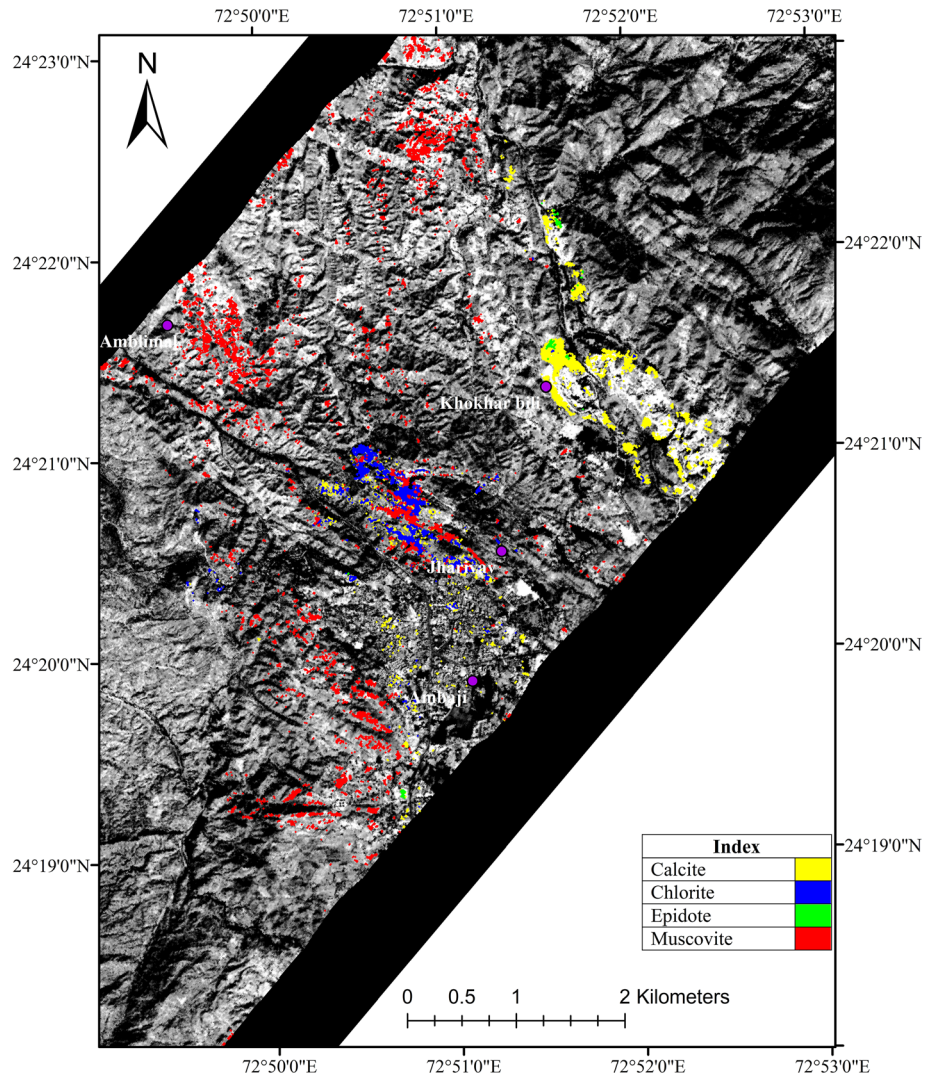
The mineral predominance map produced out of AVIRIS-NG (Fig. 5) depicts a laterally variable spatial distribution of these minerals. The pure calcite (in the form of marble) is concentrated in the NW–SE orientation for a length of 2 km near the Khokhar Bili village. The host rock in this segment is calcareous meta-sediments of Ajabgarh series of Delhi system (Heron and Ghosh 1938; Deb 1980). The chlorite, similar to calcite, is spatial present in same orientation and shows more concentration in the chloritic hornfels and diopside forsterite marble host rock around Jharivav (Deb 1980). The muscovite however on the

contrary shows more scattered signature with its distribution in south, western and northwestern parts of the studied area, with relatively higher concentrations in Amblimal (Fig. 5). Muscovite is found in the host rock same as that of chlorite (i.e. chloritic hornfels and diopside forsterite marble) (Deb 1980). Nevertheless, the distribution of chlorite is restricted to a patch near Jharivav, whereas muscovite is scattered in a wider area (Fig. 5). Epidote, on the other hand, is present only in few patches north of Khokhar Bili village. This mineral is formed over the marble of Ajabgarh series. The host rock in this area is the calcareous meta-sediments of the Ajabgarh series (Deb 1980).

Discussion

The results show the distribution of the alteration minerals (muscovite and chlorite) and calcite/epidote. The spatial distribution of these minerals is correlatable with the proved mineral deposits, i.e. existing mine owned by Gujarat Mineral Resource Development Corporation (GMDC) area for polymetallic deposits. Moreover, the muscovite also shows its high concentration around Amblimal, which is the small ore body reported earlier by Deb et al. (2001). Similarly, the calcite is more concentrated near Khokhar Bili village which is well known for its pure marble deposits (GSI 1967, 2012a). Epidote shows its

Fig. 5 Spatial distribution of the carbonate minerals at northeast of Khokhar Bili and alteration minerals around Jharivav and Amblimal



patchy appearance near Khokhar Bili. It is occasionally associated with the marble deposits (GSI 2012b).

Based on the studies on ancient sulphide deposits and its modern analogue, model proposed for explaining genesis of Volcanogenic Massive Sulfide (VMS) deposits, such deposits are deposited in submarine environment due to the convection of the seawater (Deb 1979, 1980; Galley 1993; Galley et al. 2007; Large 1992; Ross and Mercier-Langevin 2014; Tiwary and Deb 1997). During the process of formation of VMS deposits, the cold seawater percolates down through the fractures in the volcanic sequences. With increase in depth, the temperature of the seawater increases and simultaneously pH decreases; this leads to leaching of the metal elements from the host rock. Subsequently, these metals are transported upward and deposited at or near sea floor by the fluid. During this convection journey, the fluid will interact with the host rock which will result in the alteration of the feldspar in felsic volcanic rocks to white mica. In cases with further increase in temperature, the host

rock (felsic and mafic volcanic rocks) will alter to the chlorite (Galley 1993; Galley et al. 2007; Herzig and Hannington 1995; Large 1992; Ross and Mercier-Langevin 2014; Tiwary and Deb 1997). These convections are the major responsible factor for the alteration of the host rock to VMS (Galley 1993; Galley et al. 2007; Herzig and Hannington 1995; Large 1992; Ross and Mercier-Langevin 2014; Tiwary and Deb 1997).

The deposits in Ambaji–Deri region are believed to have been deposited under submarine condition (Deb 1979, 1980; Tiwary and Deb 1997). The ore metals are thought to be derived from the then basalt, which is now metamorphosed to the amphibolite, due to the result of the basalt-seawater interaction. (Deb, 1979, 1980). (Tiwary and Deb 1997) have proposed the hydrothermal alteration model for the Deri massive sulphide deposit in which the felsic and mafic volcanic rocks were altered by the basalt-seawater interaction. The model suggests that the cold seawater percolates through warmer and permeable felsic

volcanic rock. As a result, felsic volcanic rock got altered into quartz-sericite and when the temperature reached to 250 °C, it got converted into chlorite-sericite with the addition of Mg. With deeper circulation, it leached Fe and Mg. Subsequently altering the previously formed chlorite assemblages into the Biotite-Chlorite-Sericite facies (Tiwary and Deb 1997).

Apart from polymetallic deposits, lenses of economic marble deposition are also common in this area (Deb 1979, 1980; GSI 2012a). This marble deposition is made up of recrystallized calcite and is believed to be deposited in near shore transitional shelf environment (Deb 1980; GSI 2012a). In the present airborne hyperspectral study, we have mapped the distribution of these marble deposits, based on the absorption feature of the calcite, i.e. at 2330 nm. The observed spatial distribution matches well with known mineral mines and deposits in the Ambaji-Deri region (Fig. 5). Further, it should be noted that since epidote and chlorite are spectrally similar minerals (Neal et al. 2018), it is difficult to differentiate between the two at many places.

Conclusion

In the present study, we successfully illustrate the application of hyperspectral remote sensing in mapping mineral alterations, which aid in hunting newer mineral deposits. The calcite, muscovite and chlorite have been shown to be matching with the ground geological records, whereas epidote shows patchy occurrences. However, due to spectral similarities between epidote and chlorite, it is difficult to differentiate between the two only on the basis of hyperspectral studies and without being aided by geochemical analysis. Nevertheless, hyperspectral technique provides powerful tool for mapping mineral alteration to mineral deposits. This enables scrutiny of a wider area of interest to being narrowed down for first-hand field investigations.

Acknowledgement SPP would like to thank DG and Director ISR for encouragement and support. The paper forms part of ongoing AMBAJI research project of Government of Gujarat. We would like to thank ISRO-SAC for providing the AVIRIS-NG data for research purpose.

References

- Abrams, M. (2000). The advanced spaceborne thermal emission and reflection radiometer (ASTER): Data products for the high spatial resolution imager on NASA's Terra platform. *International Journal of Remote Sensing*, 21(5), 847–859.
- Amato, U., Cavalli, R. M., Palombo, A., Pignatti, S., & Santini, F. (2009). Experimental approach to the selection of the components in the minimum noise fraction. *IEEE Transactions on Geoscience and Remote Sensing*. <https://doi.org/10.1109/TGRS.2008.2002953>
- Bharti, R., Kalimuthu, R., & Ramakrishnan, D. (2015). Spectral pathways for exploration of secondary uranium: An investigation in the desertic tracts of Rajasthan and Gujarat India. *Advances in Space Research*, 56(8), 1613–1626. <https://doi.org/10.1016/j.asr.2015.07.015>
- Bharti, R., & Ramakrishnan, D. (2014). In *Geoscience and remote sensing symposium (IGARSS), 2014 IEEE international*, (pp 2902–2905).
- Bhattacharya, S., Majumdar, T. J., Rajawat, A. S., Panigrahy, M. K., & Das, P. R. (2012). Utilization of Hyperion data over Dongargarh, India, for mapping altered/weathered and clay minerals along with field spectral measurements. *International Journal of Remote Sensing*, 33(17), 5438–5450. <https://doi.org/10.1080/01431161.2012.661094>
- Boardman, J. W. (1994). Geometric mixture analysis of imaging spectrometry data. In *Geoscience and remote sensing symposium, 1994. IGARSS '94. Surface and atmospheric remote sensing: technologies, data analysis and interpretation., international*. <https://doi.org/10.1109/IGARSS.1994.399740>.
- Boardman, J. W., Kruse, F. A., & Green, R. O. (1993). Mapping target. *Jet Propulsion*, 23, 23–26.
- Carranza, E. J. M., & Hale, M. (2002). Mineral imaging with Landsat Thematic mapper data for hydrothermal alteration mapping in heavily vegetated terrane. *International Journal of Remote Sensing*, 23(22), 4827–4852. <https://doi.org/10.1080/01431160110115014>
- Crósta, A. P., De Souza Filho, C. R., Azevedo, F., & Brodie, C. (2003). Targeting key alteration minerals in epithermal deposits in Patagonia, Argentina, using ASTER imagery and principal component analysis. *International Journal of Remote Sensing*, 24(21), 4233–4240. <https://doi.org/10.1080/0143116031000152291>
- Dalton, J. B., Bove, D. J., Mladinich, C. S., & Rockwell, B. W. (2004). Identification of spectrally similar materials using the USGS Tetracorder algorithm: The calcite-epidote-chlorite problem. *Remote Sensing of Environment*, 89(4), 455–466. <https://doi.org/10.1016/j.rse.2003.11.011>
- Deb, M. (1979). Polymetamorphism of ores in Precambrian stratiform massive sulfide deposits at Ambaji-Deri Western India. *Mineralium Deposita*. <https://doi.org/10.1007/BF00201865>
- Deb, M. (1980). Genesis and metamorphism of two stratiform massive sulfide deposits at Ambaji and Deri in the Precambrian of Western India. *Economic Geology*. <https://doi.org/10.2113/gsecongeo.75.4.572>
- Deb, M., Thorpe, R. I., Krstic, D., Corfu, F., & Davis, D. W. (2001). Zircon U–Pb and galena Pb isotope evidence for an approximate 1.0 Ga terrane constituting the western margin of the Aravalli–Delhi orogenic belt, northwestern India. *Precambrian Research*, 108, 195–213.
- Gaffey, S. J. (1987). Spectral reflectance of carbonate minerals in the visible and near infrared (0.35–2.55 μm): Anhydrous carbonate minerals. *Journal of Geophysical Research*. <https://doi.org/10.1029/JB092iB02p01429>
- Galley, A. G. (1993). Characteristics of semi-conformable alteration zones associated with volcanogenic massive sulphide districts. *Journal of Geochemical Exploration*. [https://doi.org/10.1016/0375-6742\(93\)90004-6](https://doi.org/10.1016/0375-6742(93)90004-6)
- Galley, A. G., Hannington, M. D., & Jonasson, I. R. (2007). Volcanogenic massive sulphide deposits. *Special Publication*, 5, 141–161.
- Goetz, A. F. H. (2009). Three decades of hyperspectral remote sensing of the Earth: A personal view. *Remote Sensing of*

- Environment*, 113(1), S5–S16. <https://doi.org/10.1016/j.rse.2007.12.014>
- González, C., Resano, J., Mozos, D., Plaza, A., & Valencia, D. (2010). FPGA Implementation of the pixel purity index algorithm for remotely sensed hyperspectral image analysis. *Eurasip Journal on Advances in Signal Processing*. <https://doi.org/10.1155/2010/969806>
- Graham, G. E., Kokaly, R. F., Kelley, K. D., Hoefen, T. M., Johnson, M. R., & Hubbard, B. E. (2017). Airborne hyperspectral surveying as a tool for mineral exploration at high latitudes: a pilot study over porphyry Cu deposits, eastern Alaska Range, Alaska. In *14th SGA Biennial Meeting* (Vol. 3, pp. 1077–1080).
- Green, A. A., Berman, M., Switzer, P., & Craig, M. D. (1988). A Transformation for ordering multispectral data in terms of image quality with implications for noise removal. *IEEE Transactions on Geoscience and Remote Sensing*, 26(1), 65–74. <https://doi.org/10.1109/36.3001>
- GSI. (1967). Geological survey of India geological mapping in parts of Chamba District. Unpublished.
- GSI. (2012a). Geology and mineral resources of Gujarat. Unpublished.
- GSI. (2012b). Use of hyperspectral remote sensing data for the search of mineralised provinces/areas in Precambrian Terrain. Unpublished.
- Gupta S N, Arora Y K, Mathur R K, Iqbaludin p, Sahai T N, & Sharma S B. (1980). Lithostratigraphic map of Aravalli region. Kolkata.
- Harraden, C. L., McNulty, B. A., Gregory, M. J., & Lang, J. R. (2013). Shortwave infrared spectral analysis of hydrothermal alteration associated with the Pebble porphyry copper-gold-molybdenum deposit, Iliamna Alaska. *Economic Geology*, 108(3), 483–494. <https://doi.org/10.2113/econgeo.108.3.483>
- Heron, A. M., & Ghosh, P. K. (1938). Geology of Palampur, Danta and parts of Idar states. Record of Geological Survey of India.
- Herzig, P. M., & Hannington, M. D. (1995). Polymetallic massive sulfides at the modern seafloor A review. *Ore Geology Reviews*, 10(10), 95–115.
- Hunt, G. R. (1979). Near-infrared (1.3–2.4 μm) spectra of alteration minerals—Potential for use in remote sensing. *Geophysics*, 44(12), 197–198.
- Incorporated Research Systems. (2004). ENVI User's guide, (September), (pp. 1–1150).
- Khanna, S., Santos, M. J., Ustin, S. L., Shapiro, K., Haverkamp, P. J., & Lay, M. (2018). Comparing the potential of multispectral and hyperspectral data for monitoring oil spill impact. *Sensors*. <https://doi.org/10.3390/s18020558>
- Kokaly, R. F., Hoefen, T. M., Graham, G. E., Kelley, K. D., Johnson, M. R., Hubbard, B. E., et al. (2016). Mineral information at micron to kilometer scales: Laboratory, field, and remote sensing imaging spectrometer data from the orange hill porphyry copper deposit, Alaska, USA. In *International geoscience and remote sensing symposium (IGARSS)*, 2016–Nov.(pp. 5418–5421). <https://doi.org/10.1109/IGARSS.2016.7730411>
- Krishna Mohan, B., & Porwal, A. (2015). Hyperspectral image processing and analysis. *Current Science*, 108(5), 833–841.
- Kruse, F. A. (1988). Use of airborne imaging spectrometer data to map minerals associated with hydrothermally altered rocks in the northern grapevine mountains, Nevada, and California. *Remote Sensing of Environment*. [https://doi.org/10.1016/0034-4257\(88\)90004-1](https://doi.org/10.1016/0034-4257(88)90004-1)
- Kruse, F. A., Lefkoff, A. B., Boardman, J. W., Heidebrecht, K. B., Shapiro, A. T., Barloon, P. J., & Goetz, A. F. H. (1993). The spectral image processing System (SIPS) interactive visualization and analysis of imaging spectrometer data. *Remote Sensing of Environment*, 44, 145–163.
- Laakso, K., Middleton, M., Heinig, T., Bärs, R., & Lintinen, P. (2018). Assessing the ability to combine hyperspectral imaging (HSI) data with mineral liberation analyzer (MLA) data to characterize phosphate rocks. *International Journal of Applied Earth Observation and Geoinformation*, 69, 1–12. <https://doi.org/10.1016/j.jag.2018.02.018>
- Laakso, K., Peter, J. M., Rivard, B., & White, H. P. (2016). Short-wave infrared spectral and geochemical characteristics of hydrothermal alteration at the Archean Izok Lake Zn–Cu–Pb–Ag volcanogenic massive sulfide deposit, Nunavut, Canada: Application in exploration target vectoring. *Economic Geology*. <https://doi.org/10.2113/econgeo.111.5.1223>
- Laakso, K., Rivard, B., Peter, J. M., White, H. P., Maloley, M., Harris, J., & Rogge, D. (2015). Application of airborne, laboratory, and field hyperspectral methods to mineral exploration in the Canadian arctic: Recognition and characterization of volcanogenic massive sulfide-associated hydrothermal alteration in the Izok Lake Deposit Area Nunavut. *Economic Geology*. <https://doi.org/10.2113/econgeo.110.4.925>
- Large, R. R. (1992). Australian volcanic-hosted massive sulfide deposits: Features, styles, and genetic models. *Economic Geology*. <https://doi.org/10.2113/gsecongeo.87.3.471>
- Laukamp, C., Cudahy, T., Thomas, M., Jones, M., Cleverley, J. S., & Oliver, N. H. S. (2011). Hydrothermal mineral alteration patterns in the Mount Isa Inlier revealed by airborne hyperspectral data. *Australian Journal of Earth Sciences*, 58(8), 917–936. <https://doi.org/10.1080/08120099.2011.571287>
- Li, Z., Yang, R., Dang, F., Du, P., Zhang, X., Tan, B., et al. (2012). A review on the geological applications of hyperspectral remote sensing technology. *Workshop on Hyperspectral Image and Signal Processing, Evolution in Remote Sensing*. <https://doi.org/10.1109/WHISPERS.2012.6874235>
- Luo, G., Chen, G., Tian, L., Qin, K., & Qian, S. E. (2016). Minimum noise fraction versus principal component analysis as a preprocessing step for hyperspectral imagery denoising. *Canadian Journal of Remote Sensing*, 42(2), 106–116. <https://doi.org/10.1080/07038992.2016.1160772>
- Mars, J. C., & Rowan, L. C. (2006). Regional mapping of phyllic- and argillic-altered rocks in the zagros magmatic arc, Iran, using advanced spaceborne thermal emission and reflection radiometer (ASTER) data and logical operator algorithms. *Geosphere*, 2(3), 161–186. <https://doi.org/10.1130/GES00044.1>
- Mauger, A. J., Keeling, J. L., & Huntington, J. F. (2007). Alteration mapping of the Tarcoola Goldfield (South Australia) using a suite of hyperspectral methods. *Applied Earth Science*, 116(1), 2–12. <https://doi.org/10.1179/174327507X167028>
- Mishra, B. (2015). Chapter 22 precambrian metallic mineralization in India. *Geological Society, London, Memoirs*, 43(1), 327–337.
- Neal, L. C., Wilkinson, J. J., Mason, P. J., & Chang, Z. (2018). Spectral characteristics of propylitic alteration minerals as a vectoring tool for porphyry copper deposits. *Journal of Geochemical Exploration*, 184, 179–198. <https://doi.org/10.1016/j.gexplo.2017.10.019>
- Nidamanuri, R. R., & Ramiya, A. M. (2013). Spectral identification of materials by reflectance spectral library search. *Geocarto International*, 29(6), 609–624. <https://doi.org/10.1080/10106049.2013.821175>
- Nidamanuri, R. R., & Ramiya, A. M. (2014). Spectral identification of materials by reflectance spectral library search. *Geocarto International*. <https://doi.org/10.1080/10106049.2013.821175>
- Porwal, A., Carranza, E. J. M., & Hale, M. (2006). Tectonostratigraphy and base-metal mineralization controls, Aravalli province (western India): New interpretations from geophysical data analysis. *Ore Geology Reviews*. <https://doi.org/10.1016/j.oregeorev.2005.10.003>

- Pour, A. B., & Hashim, M. (2012). Identifying areas of high economic-potential copper mineralization using ASTER data in the Urumieh–Dokhtar volcanic belt Iran. *Advances in Space Research*, 49(4), 753–769. <https://doi.org/10.1016/j.asr.2011.11.028>
- Pour, A. B., & Hashim, M. (2015). Structural mapping using PALSAR data in the central gold belt peninsular Malaysia. *Ore Geology Reviews*, 64(1), 13–22. <https://doi.org/10.1016/j.oregeorev.2014.06.011>
- Pour, A. B., Hashim, M., Hong, J. K., & Park, Y. (2017). Lithological and alteration mineral mapping in poorly exposed lithologies using Landsat-8 and ASTER satellite data: North-eastern Graham Land Antarctic Peninsula. *Ore Geology Reviews*. <https://doi.org/10.1016/j.oregeorev.2017.07.018>
- Ramakrishnan, D., & Bharti, R. (2016). Hyperspectral remote sensing and geological applications. *Current Science*, 108, 879–891.
- Ross, P. S., & Mercier-Langevin, P. (2014). Igneous rock associations 14. The volcanic setting of VMS and SMS deposits: A review. *Geoscience Canada*. <https://doi.org/10.12789/geocanj.2014.41.045>
- Sabins, F. (1999). Remote sensing for mineral exploration. *Ore Geology Reviews*, 14(3–4), 157–183. [https://doi.org/10.1016/S0169-1368\(99\)00007-4](https://doi.org/10.1016/S0169-1368(99)00007-4)
- Shaw, G. A., & Burke, H. K. (2003). Spectral imaging for remote sensing. *Lincoln Laboratory Journal*, 14(1), 3–28.
- Swayze, G. A., Clark, R. N., Goetz, A. F. H., Livo, K. E., Breit, G. N., Kruse, F. A., et al. (2014). Mapping advanced argillic alteration at Cuprite, Nevada, using imaging spectroscopy. *Economic Geology*. <https://doi.org/10.2113/econgeo.109.5.1179>
- Taylor, P., Gens, R., & Genderen, J. L. V. A. N. (2007). Review Article SAR interferometry—issues, techniques, applications. *International Journal of Remote Sensing*, 17, 37–41.
- Tiwary, A., & Deb, M. (1997). Geochemistry of hydrothermal alteration at the Deri massive sulphide deposit, Sirohi district, Rajasthan. *NW India. Journal of Geochemical*, 59(59), 99–121.
- van der Meer, F. D., van der Werff, H. M. A., van Ruitenbeek, F. J. A., Hecker, C. A., Bakker, W. H., Noomen, M. F., et al. (2012). Multi- and hyperspectral geologic remote sensing: A review. *International Journal of Applied Earth Observation and Geoinformation*. <https://doi.org/10.1016/j.jag.2011.08.002>
- Wu, X., Huang, B., Plaza, A., Li, Y., & Wu, C. (2014). Real-time implementation of the pixel purity index algorithm for end-member identification on GPUs. *IEEE Geoscience and Remote Sensing Letters*, 11(5), 955–959. <https://doi.org/10.1109/LGRS.2013.2283214>

Publisher's Note Springer Nature remains neutral with regard to jurisdictional claims in published maps and institutional affiliations.